Performance Comparisons Of A Unitary Split System Using Microchannel and Fin-Tube Outdoor Coils, Part I: Heating Tests

J. H. Kim
Purdue University

E. A. Groll
Purdue University

R6-8

PERFORMANCE COMPARISONS OF A UNITARY SPLIT SYSTEM USING MICROCHANNEL AND FIN-TUBE OUTDOOR COILS, PART II: HEATING TEST

Jun-Hyeung Kim and Eckhard A. Groll

Purdue University
Ray W. Herrick Laboratories
West Lafayette, IN 47907, USA

ABSTRACT

This two-part paper investigates the performance of a unitary split system using microchannel heat exchangers instead of the conventional fin-tube designs as the outdoor coil for air conditioning and heat pumping applications. Microchannel heat exchangers are said to offer higher performance per unit weight and reduce refrigerant charge in vapor compression systems, but little is known about their performance characteristics in unitary equipment, especially with respect to the frosting and defrosting characteristics during heat pump mode.

A commercially available 3-ton heat pump with a conventional outdoor heat exchanger serves as the baseline system. Performance tests were conducted with the conventional outdoor coil and after replacing the outdoor coil with custom made microchannel heat exchangers. The tests consisted of standard ARI cooling and heating/defrosting tests. The Part I paper describes the microchannel heat exchanger configurations and presents the results obtained during the cooling tests. The Part II paper presents the results of the heating/defrosting tests.

NOMENCLATURE

C_p	Specific heat ($kJ \cdot kg^{-1} \cdot K^{-1}$)
h	Specific enthalpy ($kJ \cdot kg^{-1}$)
$\dot{m}$	Mass flow rate ($kg \cdot s^{-1}$)
Q	Capacity (kW)
W	Power (kW)
T	Temperature (C)
t	Time (s)

Subscripts:

a	air
c	condensing
h	heating
i	inlet
o	outlet
m	mean
r	refrigerant
comp	compressor

INTRODUCTION

In the Part I paper (Kim and Groll 2002), the layout and design of the microchannel heat exchangers as they were used to replace the conventional outdoor coil were described in detail, and the results of the system performance tests in cooling mode were presented. It was concluded that the microchannel heat exchangers outperform the baseline coil in cooling mode with respect to cooling capacity and EER even though the microchannel heat exchangers had 23% less face area and 32% less inside (refrigerant- side) volume than the baseline coil.

It is known that microchannel heat exchanger, which operate at wet conditions, i.e., in which the water vapor of the humid air condenses on the fin surface, may have a drainage problem. Placed horizontally, the condensed water is being held up in the corrugated fin bends and on the flat tubes. The standing water may cause funny smells and disables the humidity control typically achieved by evaporator air coils. Better drainage of the water can usually be achieved if the microchannel heat exchanger is placed vertically. However, in this case some of the condensed water tends to collect between the corrugated fins, forming a water bridge, or between the louvered fins leading to a louver blockage. Osada et al. (2001) reported that with hydrophilic-coated fins, the drainage can be improved because the condensed water is easily dragged out through the corrugated fins by shear stress of the air and drains down along the rear end of the flat tubes. It is also reported that in cases where the air is flowing normal to the face area, a windward inclination of the microchannel heat exchanger with a fin spacing of 3 mm and a fin depth of 58 mm promotes the water drainage of the coil. In this case, gravity is utilized to pull out the condensed water, which drains down along the front end of the flat tubes. However, little is known about the effect of frost formation on the performance of microchannel heat exchangers, as it is quite common to a residential heat pump in winter operation.

This paper discusses the characteristics of microchannel heat exchangers as the outdoor coil in a residential heat pump system operating in heating mode with frost formation. The overall system performance, the heating/frosting time periods, and the defrost time periods are presented.

EXPERIMENTAL PROCEDURES

The same test stand, test coils, and measuring instrumentation that were used for the cooling tests (Kim and Groll 2002) were also used for the heating tests. The heating tests were conducted at ARI Test "35" conditions (35±0.5°F ODDB, 33±0.5°F ODWB, and 70±0.5°F IDDB) with an indoor air volumetric flow rate of 1200 CFM. After the baseline heating tests were completed, the baseline outdoor heat exchanger was replaced with four different microchannel heat exchanger configurations. These configurations differ in their number of fins per inch, i.e., 15 FPI versus 20 FPI, and their orientation, i.e., vertically placed versus 15° slanted towards windward. Additional details of the microchannel heat exchanger configurations are presented in the Part 1 paper (Kim and Groll 2002). Each heating test was repeated at least two times for redundancy and repeatability. Since the outdoor coil operates as an evaporator in heating mode, the refrigerant flowed upwards through the microchannel heat exchangers to maintain a better refrigerant distribution. All data were recorded in five seconds intervals.

Data Reduction

To analyze the heating tests, only the air enthalpy method is permissible due to the nature of the cyclical tests at ARI Test "35" conditions. Since the heating tests are transient, the average heating capacity is calculated by the following equations:

$$\overline{Q}_{h,a} = \int_{t_1}^{t_2} Q_{h,a}(t)\, dt \Big/ \left(t_2 - t_1\right)$$

$$Q_{h,a}(t) = \dot{m}_a(t)\ C_{p,a,m}(t)\ \left(T_{a,o}(t) - T_{a,o}(t)\right) z$$

where t_1 and t_2 are the time of the first defrost termination and the next defrost termination, respectively. $Q_{h,a}(t)$ is the local heating capacity. The average power consumptions of the outdoor fan and the compressor are calculated by the following equations:

$$\overline{W}_{h,fan} = \int_{t_1}^{t_2} W_{h,fan}(t)\, dt \Big/ (t_2 - t_1)$$

$$\overline{W}_{h,comp} = \int_{t_1}^{t_2} W_{h,comp}(t)\, dt \Big/ (t_2 - t_1)$$

where $W_{h,fan}(t)$ and $W_{h,comp}(t)$ are the local power consumptions of the outdoor fan and the compressor, respectively. The Trapezoid Rule of numerical integration that has the global error of $O(\Delta t^2)$ was applied to perform the integrations. The overall system performances such as COP and EER were determined by the following equations:

$$COP_h = \overline{Q}_{h,a} \Big/ \left(\overline{W}_{h,fan} + \overline{W}_{h,comp}\right)$$

$$EER = 3.412\ COP_h$$

HEATING TEST RESULTS

This section presents the performance characteristics of the microchannel heat exchangers as an outdoor coil during heating/frosting and defrosting conditions, and discusses the effects of using different orientation and FPI of the microchannel heat exchanger on heating capacities, power consumptions, and system efficiencies.

Heating/Frosting Time and Defrosting Time

One complete heat pump cycle consists of a heating/frosting period and a defrosting period. Table 1 presents the heat/frosting time periods and the defrosting time periods for three continuous heat pump cycles of the systems with the vertically placed microchannel heat exchangers as the outdoor coil. It can be seen from Table 1 that the heating/frosting time period decreases and the defrosting time period increases with each heat pump cycle. This is due to the fact that some condensate remains on the fins after each defrost period. During the defrost period, the outdoor fan remains off and thus, there is no shear force working on the condensate film that may help to drain the condensate from the fin surface. The remaining condensate immediately freezes during the next heating/frosting period and quickly blocks the air passages. This can be observed in Figure 1, which shows a photograph of a vertically-placed microchannel heat exchanger directly after completion of a defrost period. Several remaining water droplets are clearly visible. As a result, the heating/frosting time period gets shorter and the defrosting time period gets longer with each heat pump cycle. This degrades the heating capacities as well as the system performance with each heat pump cycle, as shown in Table 2.

Initially, it was expected that an inclination of the microchannel heat exchanger could help to drain the condensate from the fin surface by utilizing the gravitational force. However, it turned out that a 15° windward inclination of the microchannel heat exchanger did not make a significant difference in water drainage. This indicates that the surface tension on the water bridge condensate is greater than the tangential force of gravity on the condensate using a 15° inclination of the tested microchannel heat exchanger. As a result, some of the condensate still remains between the fins. It can be seen from Table 1 and 2 that the inclined heat exchangers show the same trends as the vertically placed heat exchangers. The heating/frosting time period decreases, the defrosting time period increases, and the heating capacity and the system performance decrease with each heat pump cycle.

Frost line on each panel of the microchannel heat exchanger

It was observed that most of the frost is concentrated towards the lower part of the microchannel panels, and that more frost is located on the left and right side of each panel rather than in the middle of the panel. The frost formation on four panels of the vertically placed microchannel heat exchangers with 15 FPI are shown in Figure 2. It is assumed that the baffle that was installed in the middle of the bottom header of each microchannel heat exchanger panel with the intention of providing a better refrigerant distribution results in a slightly uneven refrigerant distribution. Most of the refrigerant flows into the side channels of each panel, while somewhat less refrigerant flows into the middle channels. This implies that redesigning the baffle may further improve the refrigerant distribution. The same trends were also observed with respect to the frost formation on the angularly placed microchannel heat exchangers.

Table 1: Comparisons of the heating/frosting and defrosting time periods for three continuous heat pump cycles

System	Heating/frosting time			Defrosting time		
	1st cycle	2nd cycle	3rd cycle	1st cycle	2nd cycle	3rd cycle
Baseline	85 min 35 sec	N/A	N/A	5 min	N/A	N/A
PHMV20	29 min 50 sec	30 min 10 sec	28 min 10 sec	3 min	3 min 30 sec	3 min 55 sec
PHMA20	25 min 15 sec	24 min	24 min 45 sec	2 min 30 sec	2 min 40 sec	2 min 55 sec
PHMV15	35 min 35 sec	33 min 20 sec	32 min 10 sec	2 min 5sec	3 min 5 sec	3 min 25 sec
PHMA15	28 min 50 sec	26 min 30 sec	24 min 10 sec	2 min 30 sec	2 min 55 sec	3 min

* Baseline, PHMV20, PHMA20,PHMV15, and PHMA15 data come from PHB-1, PHMV20-1,PHMA20-1, PHMV15-1, and PHMA15-1 data, respectively.

Table 2: Comparisons of the heating capacity and the system EER for three continuous heat pump cycles

System	Heating capacity (kW)			EER (Btu/hr/W)		
	1st cycle	2nd cycle	3rd cycle	1st cycle	2nd cycle	3rd cycle
Baseline	7.02157	N/A	N/A	9.37546	N/A	N/A
PHMV20	6.075	5.929	5.692	8.125	7.941	7.634
PHMA20	6.443	6.280	6.090	8.536	8.290	8.048
PHMV15	6.660	6.469	6.174	9.043	8.800	8.470
PHMA15	6.482	6.147	5.922	8.563	8.345	8.123

* Baseline, PHMV20, PHMA20,PHMV15, and PHMA15 data come from PHB-1, PHMV20-1,PHMA20-1, PHMV15-1, and PHMA15-1 data, respectively

Effect of orientation of the microchannel heat exchangers

The average heating capacities obtained during the five heating tests as a function of time, beginning with the startup of the unit, are shown in Figure 3. At the beginning of the initial heating/frosting time period and after each defrost period, the average heating capacity gradually increases until it reaches a maximum. At this point the frost formation starts to degrade the performance and the average heating capacity gradually decreases as time moves on until the frost accumulation forces the initiation of the defrost cycle. At this point, the average heating capacity steeply decreases.

Overall, the PHMA20 (Performance-Heating-Microchannel-Angular-20 FPI) system delivers a higher average heating capacity than the PHMV20 (V = Vertical) system since the angularly placed heat exchanger has higher heat transfer characteristics than the vertically placed heat exchanger, as discussed in cooling test results of the Part 1 paper (Kim and Groll 2002). However, the PHMA20 system initiates the defrost cycle earlier than the PHMV20 system as shown in Table 1. This is mainly due to the different air flow patterns through the fins. If the air flow is more normal in the direction of the microchannel heat exchanger face area, which is the case of the PHMA20 system, the microchannel heat exchanger has more stratified air flow. This results in a faster frost growth on the fins. The faster frost growth blocks the air flow passages more quickly, and thus, results in a faster decrease of the heat transfer and system performance. This causes the PHMA20 system to initiate the defrost cycles earlier than the PHMV20 system. The PHMA20 system has three-and-a-half complete heat pump cycles and the PHMV20 system has three complete heat pump cycles, during the time period in which the baseline system has one complete cycle. It has to be noted that the baseline outdoor coil was a spine-fine heat exchanger that is known to handle significant frost accumulation before a defrosting cycle has to be initiated.

Also shown in Figure 3 are the average heating capacities of the heat pump systems with the 15 FPI microchannel heat exchanger. The PHMV15 system delivers a higher average heating capacity and performs better than the PHMA15 system, as shown in Figure 4. Unlike the microchannel heat exchangers with 20 FPI, slanting the microchannel heat exchangers with 15 FPI does not improve the heat transfer. The average heating capacity of the PHMA15 system is almost the same as that of the PHMV15 system from 0 to 1000 seconds. After 1000 seconds, the heat transfer of the angularly placed microchannel heat exchangers with 15 FPI decreases more quickly than that of the vertical placed microchannel heat exchangers with 15 FPI due to the faster growth of frost on the fins. It results in less average heating capacity and eventually contributes to an early initiation of defrost cycle as shown in Figure 3. The PHMA15 system has three complete cycles, and the PHMV15 system has two-and-a-half complete cycles while the baseline system has one complete cycle.

Effect of FPI of the microchannel heat exchangers

By comparing the results of the PHMV15 system to the ones of the PHMV20 system it can be observed that the PHMV15 system has a longer heating/frosting time period than the PHMV20 system as shown at Table 2. This is due to the fact that the microchannel heat exchanger with 15 FPI has less density of fins per unit volume than the microchannel heat exchanger with 20 FPI. Less density of fins per unit volume means less outside surface area and lower air velocity through the fins. Lee, Kim, and Lee (1999) specifically discussed that the accumulation of frost on a flat fin increased with increasing air velocity. Thus, the 15 FPI heat exchanger had less accumulation of frost and less blockage of air flow through the fins. Therefore, the heat transfer of the microchannel heat exchanger with 15 FPI degrades more slowly than the microchannel heat exchanger with 20 FPI. Consequently, the PHMV15 system has longer heating/frosting time period. The PHMV15 system has two-and-a-half complete cycles, and the PHMV20 system has three complete cycles while the baseline system has one complete cycle. Between the PHMA15 system and the PHMA20 system, the PHMA15 system has a longer heating/frosting time period than the PHMA20 system, as shown at Table 2, for the same reasons as stated above. However, in the case of the angularly placed microchannel heat exchangers, the usage of different FPI does not change the heat transfer as much and the average heating capacity of the PHMA15 system is almost equal to the one of the PHMA20 system from 0 to 1500 seconds. A similar result was also reported in cooling test results of the Part I paper (Kim and Groll 2002), in which case the angularly placed microchannel heat exchangers with 15 and 20 FPI had a similar cooling capacity. However, switching from 15 FPI to 20 FPI has an effect on the frequency of the defrost cycle. The PHMA20 system initiates the defrost cycle earlier than the PHMA15 system due to the higher density of fins per unit volume.

CONCLUSION

The performance of a commercially available nominal 3-ton residential split system heat pump system was tested at ARI Test "35" heating conditions using five different outdoor heat exchangers. The first outdoor heat exchanger was the baseline spine-fin heat exchanger. The other four heat exchangers were vertically-placed and angularly-placed (slanted 15° toward windward) microchannel heat exchanger with 15 and 20 fins per inch. The microchannel heat exchangers had about 23% less face area and 32% less inside volume than the baseline heat exchanger.

The results show that all four microchannel heat exchanger configurations result in an average heating capacity and system performance that is lower than that of the baseline system. Of the microchannel heat exchanger configurations, the vertically installed heat exchanger with 15 FPI had the highest average heating capacity, followed by the angularly placed heat exchangers (regardless of FPI), followed by the vertically placed heat exchanger with 20 FPI. The same order also applies with respect to system performance (heating EER) since the average power consumptions of the fan and compressor do not change that much between the different systems. Among the five systems, the baseline system has the lowest frequency of defrost cycles, followed by vertically placed 15 FPI system, the vertically placed 20 FPI system, the angularly placed 15 FPI system, and the angularly placed 20 FPI system. Consequently, the angularly placed 20 FPI system has the highest risk of hurting the reliability of the system in comparison to the other systems.

The results of using different orientations of the microchannel heat exchanger with the same fins per inch are not consistent. In case of 20 FPI, the angular installation of the microchannel heat exchanger increases the average heating capacity and the system performance. In case of 15 FPI, the opposite is true. However, irregardless of the FPI, the angular installation of the microchannel heat exchanger contributes to a higher frequency of defrost cycles.

The results of using different FPI of the microchannel heat exchanger using the same orientation indicate that a switch from 20 to 15 FPI did not change the system performance for an angular orientation. When placed vertically, however, it improves the system performance. In addition, a smaller FPI always results in a lower frequency of defrost cycles. The frequency of the defrost cycles is strongly connected to how quickly the accumulated frost blocks the air flow passages between the fins.

ACKNOWLEDGEMENTS

The study was funded by ASHRAE (Project No. ASHRAE 1195-RP), and the baseline system and the microchannel heat exchangers were donated by the Trane Company and Heatcraft, Inc., respectively. The support of ASHRAE, Trane, and Heatcraft is gratefully acknowledged.

REFERENCES

Osada, H. et al, "Research on Corrugated Multi-Louvered Fins under Dehumidification," Heat Transfer-Asian Research, Vol. 30, No. 5, 2001, pp. 383-393.

Kim, J.-H., and Groll, E.A., "Performance Comparisons of a Unitary Split System Using Microchannel and Fin-Tube Outdoor Coils, Part I: Cooling Tests," Proc. Int'l Refrig. and Air Cond. Conf. at Purdue, West Lafayette, IN, July 16-19, 2002.

Lee, K. S., and Kim, W. S., 1997, "A one-dimensional model for frost formation on a cold flat surface," International Journal of Heat and Mass Transfer, Vol. 40, No. 18, pp. 4359-4365.

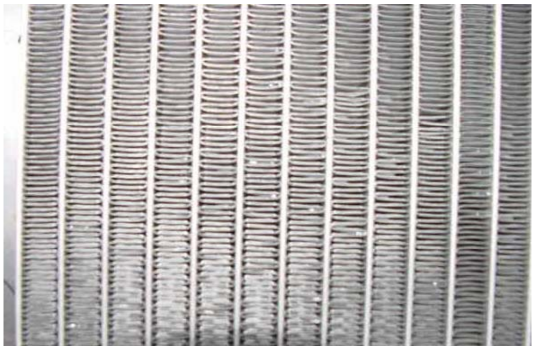

Figure 1: Remaining condensate in the vertically placed microchannel heat exchanger with 15 FPI after a defrost cycle

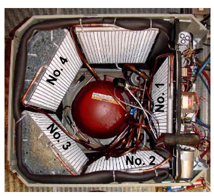

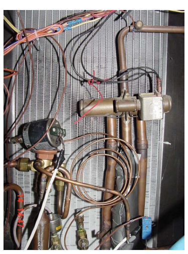

No. 1

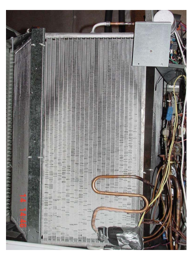

No. 2

No. 3

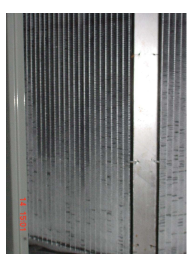

No. 4

Figure 2: Frost lines of each panel of the vertically placed microchannel heat exchangers with 15 FPI

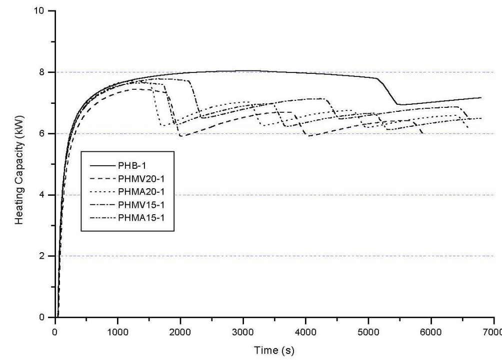

Figure 3: Average heating capacity of the heating tests

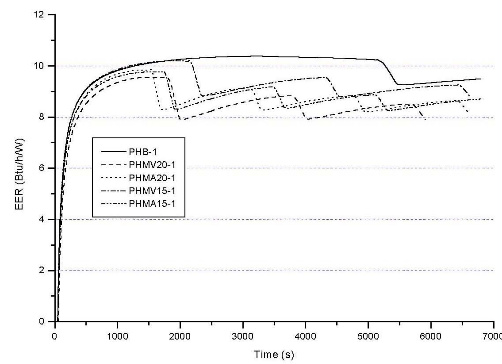

Figure 4: System performance of the heating tests